IJMMM International Journal of Minerals, Metallurgy and Materials 矿物冶金与材料学报（英文版）

Hot compressive deformation of eutectic Al–17at% Cu alloy on the interface of the Cu–Al composite plate produced by horizontal continuous casting

Jun Wang, Fan Zhao, Guoliang Xie, Jiaxuan Xu, and Xinhua Liu

Cite this article as:
Jun Wang, Fan Zhao, Guoliang Xie, Jiaxuan Xu, and Xinhua Liu, Hot compressive deformation of eutectic Al–17at% Cu alloy on the interface of the Cu–Al composite plate produced by horizontal continuous casting, *Int. J. Miner. Metall. Mater.*, 29(2022), No. 8, pp. 1578-1588. https://doi.org/10.1007/s12613-021-2276-4

International Journal of Minerals, Metallurgy and Materials
Volume 29, Number 8, August 2022, Page 1578
https://doi.org/10.1007/s12613-021-2276-4

Hot compressive deformation of eutectic Al–17at% Cu alloy on the interface of the Cu–Al composite plate produced by horizontal continuous casting

Jun Wang[1)], *Fan Zhao*[1)], *Guoliang Xie*[2)], *Jiaxuan Xu*[1)], *and Xinhua Liu*[1),✉]

1) Key Laboratory for Advanced Materials Processing (MOE), Institute for Advanced Materials and Technology, University of Science and Technology Beijing, Beijing 100083, China

2) State Key Laboratory for Advanced Metals and Materials, University of Science and Technology Beijing, Beijing 100083, China

(Received: 4 November 2020; revised: 22 February 2021; accepted: 2 March 2021)

Abstract: On the interface of the Cu–Al composite plate from horizontal continuous casting, the eutectic microstructure layer thickness accounts for more than 90% of the total interface thickness, and the deformation in rolling forming plays an important role in the quality of the composite plate. The eutectic microstructure material on the interface of the Cu–Al composite plate was prepared by changing the cooling rate of ingot solidification and the deformation in hot compression was investigated. The results show that when the deformation temperature is over 300°C, the softening effect of dynamic recrystallization of α-Al is greater than the hardening effect, and uniform plastic deformation of eutectic microstructure is caused. The constitutive equation of flow stress in the eutectic microstructure layer was established by Arrhenius hyperbolic-sine mathematics model, providing a reliable theoretical basis for the deformation of the Cu–Al composite plate.

Keywords: horizontal continuous casting; copper–aluminium composite plate; composite interface; eutectic microstructure material; hot deformation experiments; constitutive equation

1. Introduction

The Cu–Al composite plate has attracted more attention in recent years because of its advantages of copper and aluminum [1–3], such as lightweight of aluminum and high conductivity and thermal conductivity of copper [4–6]. There are many preparation methods of Cu–Al composites plate, including the explosion recombination method [7–8], rolling recombination method [9–11], compound casting method [12–13], casting and rolling recombination method [14–15], and horizontal continuous casting composite forming method [16]. Horizontal continuous casting compound forming process is as follows: copper and aluminum liquids are heated and insulated separately, with induction heating for the thermal type mold. Upon achieving the preset temperature, the copper plate is induced by the traction device for casting the copper strip, followed by the discharge of the aluminum liquid. With the effect of cooling in the crystallizer, the aluminum liquid is solidified on the copper substrate to produce a copper–aluminum bimetallic compound strip. The horizontal continuous casting composite forming method can achieve large-scale continuous production of Cu–Al composites plate due to its advantages of short technological process and excellent metallurgical bonding of composite interface [17]. However, due to brittle intermetallic compounds and the eutectic phase at the composite interface, the deformation behavior of Cu–Al composites plate prepared by horizontal continuous casting composite forming process is completely controlled by experience. The numerical simulation method is used to study the stress field distribution of Cu–Al composites plate in the forming process and optimize the parameters of the forming process, which is an effective way to realize the forming process of Cu–Al composites plate.

Wu and Liu [18] used finite element software Abaqus to simulate the rolling process of rectangular section copper-clad aluminum composite material. The simulation results showed that the single-pass reduction has the most intensive influence on the lateral spread ratio and copper sheath thickness ratio. Li *et al.* [19] used finite element software Marc to simulate the rolling process of copper clad aluminum composites. According to the research results, based on the theoretical calculation formula of rolling load for a single material, the rolling load calculation formula for bimetallic composites was proposed and the correctness of the formula was verified. Luo *et al.* [20] used 3D rigid–plastic finite element model to investigate the effect of main process parameters on the deformation behavior of copper cladding aluminum wire forming process. It suggested that the flat wire had more spread rate and uniformity of the copper layer using possible fewer passes. The above of all research in establishing the model, assuming binding constraint between the copper and aluminum layer, ignored the existence of the composite inter-

✉ Corresponding author: Xinhua Liu E-mail: Liuxinhua18@163.com

face. However, Liu *et al.* [21] found that the co-deformation of the two substrates could be realized due to the bonding effect of the composite interface by comparing the hot compression process of the Cu–Al composites plate with the metallurgical bonding interface and the no-interface Cu/Al composite sample. Therefore, the deformation behavior of the composite interface is the key factor during the forming process of the Cu–Al composites plate. However, the composite interface size is small, about 500 μm, it is difficult to study the deformation behavior of the composite interface directly in the forming process, so there are few reports on this aspect.

The composite interface of Cu–Al composites plate fabricated by horizontal continuous casting composite forming is composed of the eutectic microstructure layer and intermetallic compound [16]. Intermetallic compounds are brittle and have little plastic deformation ability. The thickness of eutectic layer accounts for more than 90% of the total thickness of the interface, the deformation behavior of the eutectic layer in the subsequent rolling process has a significant influence on the quality of Cu–Al composites plate after forming. In this paper, Al–17at% Cu alloy with the same eutectic structure as the eutectic microstructure layer of the Cu–Al composites plate fabricated by horizontal continuous casting composite forming was prepared to replace the eutectic microstructure layer by changing the cooling speed of the ingot. The thermal deformation behavior of the eutectic microstructure layer was studied by hot compression experiment, and the Arrhenius equation was used to construct the constitutive equation of the eutectic microstructure layer, which provides a solid theoretical basis for the hot forming process of Cu–Al composites plate.

2. Experimental

2.1. Preparation eutectic microstructure layer of Cu–Al composites plate by horizontal continuous casting composite forming

According to previous studies, the composite interface microstructure of Cu–Al composites plate formed by horizontal continuous casting is shown in Fig. 1. According to energy dispersive spectroscopy (EDS) analysis results in Table 1, the main composition of Cu–Al composites plate with the eutectic microstructure layer is Al–17at% Cu alloy, and the phase composition is α + θ phase.

In this experiment, Al–20at% Cu intermediate alloy was firstly prepared by using cathode copper and industrial pure aluminum in the medium frequency vacuum induction melting furnace, then Al–17at% Cu alloy was prepared by using

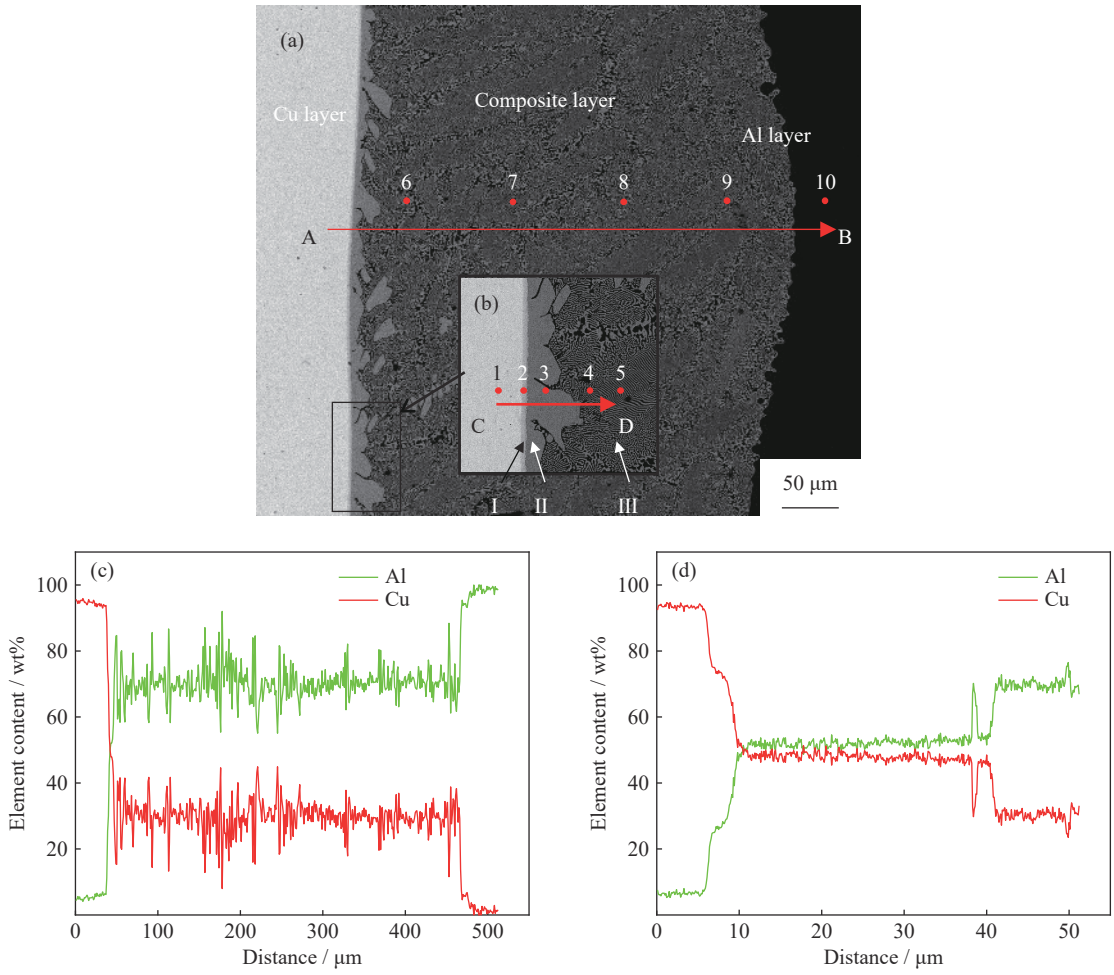

Fig. 1. Microscopic results and element distribution of the composite interface: (a, b) the microstructure of the interface; (c, d) EDS line sweep analysis results of A–B in (a) and C–D in (b).

Table 1. EDS component analysis results of points in Fig. 1

Point	Cu / at%	Al / at%	Phase	Point	Cu / at%	Al / at%	Phase
1	99.07	0.93	α-Cu	6	15.52	84.48	α + θ
2	74.38	25.62	γ	7	18.21	81.79	α + θ
3	35.23	64.77	θ	8	16.97	83.03	α + θ
4	17.22	82.78	α + θ	9	16.66	83.34	α + θ
5	17.17	82.83	α + θ	10	1.73	98.27	α-Al

intermediate alloy and industrial pure aluminum in the resistance furnace. As can be observed from the Al–Cu binary phase diagram, the melting point of the Al–17at% Cu alloy is 564.3°C, and therefore the preset temperature of the alloy was 650°C. The Al–17at% Cu alloy was completely melted and insulated for 10 min at a preset temperature. The graphite crucible containing the molten metal was removed, and the molten metal was refined and de-hybridized with the C_2Cl_6 refining agent. The graphite crucible was placed in the resistance furnace for heating the molten metal to the preset temperature and insulating it for 10 min, after which the ingots were cast and solidified under various process conditions, respectively (see Table 2 for specific process parameters). The optimum preparation process was determined by comparing the microstructure and composition of the ingots prepared under different technological conditions with the eutectic interface of the Cu–Al composites plate, which provided samples for the hot compression experiment.

Table 2. Specific process parameters of three cooling methods

No.	Cooling method
1	Air cooling
2	3 mm graphite gaskets between the cast mold and the water-cooled base plate
3	The cast mold placed directly on the water-cooled base plate

2.2. Test analysis method

10 mm × 10 mm × 20 mm samples were taken from Al–17at% Cu alloy ingot prepared by wire cutting method under different technological conditions. After sandpaper polishing and mechanical polishing, Phenom ProX scanning electron microscope was used to observe the microstructure and composition of the samples. The ϕ8 mm × 15 mm cylindrical sample was prepared using the wire cutting method to process the ingot prepared by the best process. Gleeble-1500 thermal simulator was used to conduct thermal compression experiments on the cylindrical samples. The experimental conditions were as follows: the deformation temperatures of room temperature, 200, 250, 300, 350, and 400°C, the strain rates of 0.01, 0.1, and 1 s^{-1}, and the total compression deformation of 70%. The experimental data was collected automatically by the computer system of the thermal simulation testing machine. The fracture morphology of the sample was observed with Phenom ProX scanning electron microscope, and JSM-7900F field emission scanning electron microscope was used to observe the microstructure of the deformed specimens. The true stress–true strain curve was drawn according to the experimental results of thermal compression, and the rheological behavior constitutive relation of the eutectic microstructure layer was established.

3. Results and discussion

3.1. Microstructure and composition

The microstructures of ingot prepared by different processes are shown in Fig. 2. As can be seen from the figure, the solidification organization of the Al–17at% Cu alloy comprises a certain amount of incipient intermetallic compound phase θ-$CuAl_2$ and a dense lamellar eutectic organization, which is regarded as a typical hypereutectic organization. There are mostly obvious corners in the incipient θ-$CuAl_2$ phase, which demonstrates that in the Al–17at% Cu alloy, the incipient intermetallic compound phase θ-$CuAl_2$ during the growth process exhibits a small planar growth. As the cooling rate increases, the θ-$CuAl_2$ phase is transformed from long slat to short rectangle. Meanwhile, the increase in cooling rate affects the gradient of solute concentration distribution in the liquid phase at the front of the dendrites during solidification, which further influences the nucleation and growth of the eutectic organization, leading to a significant refinement of the eutectic organization and the appearance of a large number of eutectic clusters.

By comparing with the eutectic microstructure layer of the Cu–Al composites plate by horizontal continuous casting composite forming, it is found that the grain size and growth direction of the sample prepared by the No. 3 process are the same as those of the eutectic microstructure layer. Table 3 shows the EDS analysis results of points in Fig. 2(d), the phase composition of the ingot sample prepared by the No. 3 process is α + θ phase, which is also consistent with the eutectic microstructure layer phase composition of Cu–Al composites plate. Therefore, the casting ingot prepared by the No. 3 process can be used to replace the eutectic microstructure layer of Cu–Al composites plate by the horizontal continuous casting composite forming to study the hot compression deformation behavior of the eutectic microstructure layer.

3.2. Compression deformation behavior

During the hot compression experiment, it was found that the eutectic microstructure layer broke when the deformation

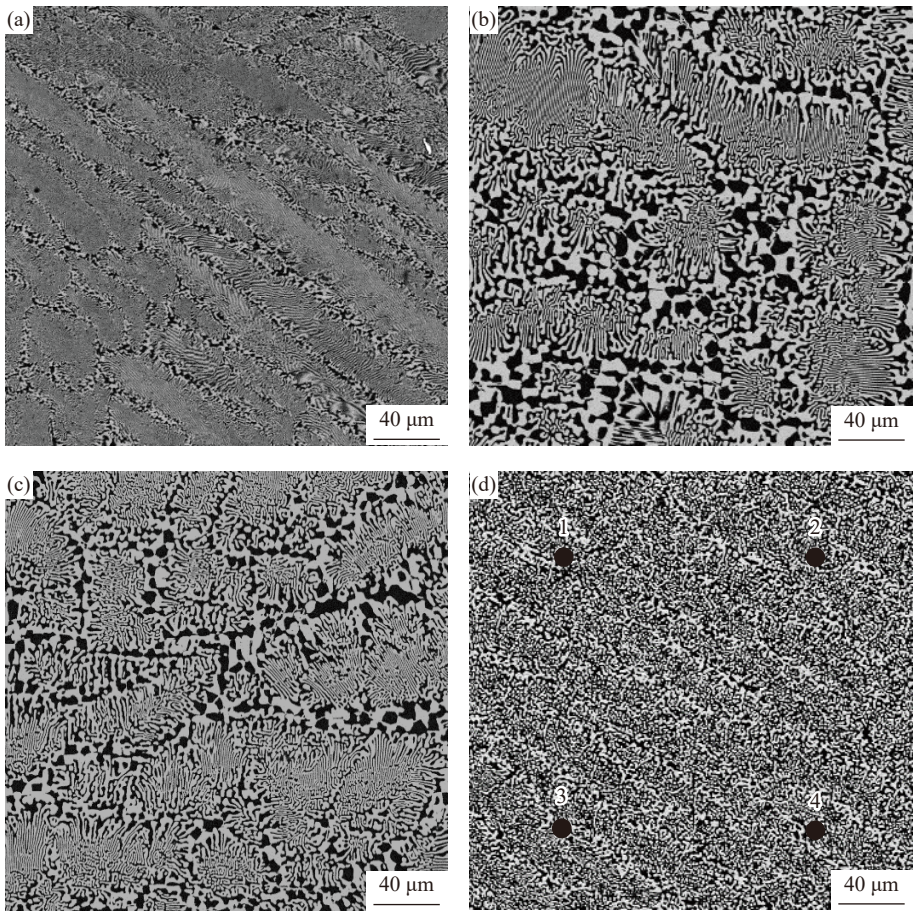

Fig. 2. (a) Eutectic microstructure layer and the microstructure of the samples prepared by different cooling methods: (b) No. 1, (c) No. 2, and (d) No. 3.

Table 3. EDS analysis results of points in Fig. 2(d)

Point	Cu / at%	Al / at%	Phase
1	17.2	82.8	α + θ
2	15.3	84.7	α + θ
3	16.5	83.5	α + θ
4	18.6	81.4	α + θ

temperature was low and the strain rate was high. The fracture morphology of the sample is shown in Fig. 3. The fracture morphology (Fig. 3(a) and (b)) has cleavage steps and river patterns, which are typical micro characteristics of cleavage fractures. It shows that the fracture mode of the eutectic microstructure layer is brittle fracture when the deformation temperature is lower than 200°C. The fracture morphology shown in Fig. 3(c) is characterized by a quasi-cleavage fracture with tearing edge in addition to the cleavage step and river pattern. The fracture morphology changes with the increase of deformation temperature, indicating that when the deformation temperature is higher than 250°C, the fracture mode changes from brittle fracture to ductile fracture, and the plastic deformation ability of the eutectic microstructure increases.

When the deformation temperature is greater than 300°C, the eutectic microstructure layer produces uniform plastic deformation without a noticeable "bulge" phenomenon. The deformed sample was cut along the axial direction, and the microstructure of the deformed eutectic microstructure layer was observed. The microstructure of the eutectic microstruc-

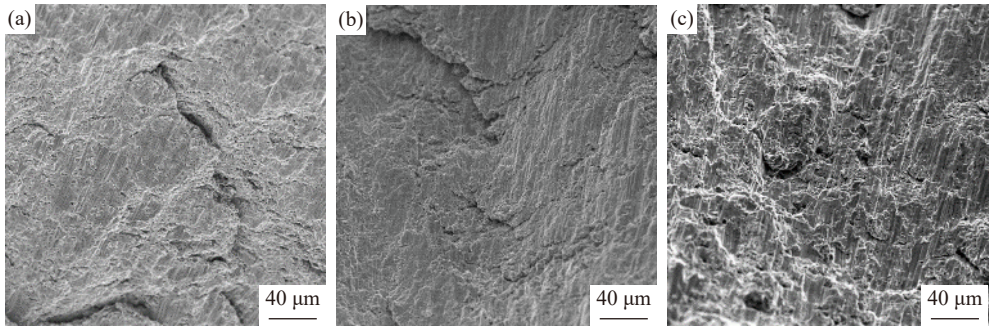

Fig. 3. Fracture morphologies of eutectic microstructure layer after compression deformation under different conditions: (a) room temperature, 1 s^{-1}; (b) 200°C, 1 s^{-1}; (c) 250°C, 1 s^{-1}.

ture layer under the deformation condition of 350°C and 0.01 s^{-1} is shown in Fig. 4. When the deformation temperature was 350°C, the $CuAl_2$ phase was crushed under the action of stress and dispersed in the α-Al phase. The complete recrystallization of α-Al results in the softening of the eutectic microstructure layer and a sharp decrease in the degree of work hardening, and the composite eutectic interface shows good plastic deformation ability.

The eutectic microstructure layer microstructure under different strain rates at the deformation temperature of 350°C is shown in Fig. 5. When the temperature is fixed, the size of dynamically recrystallized grains decreases gradually with the increase of strain rate. This is due to the driving force of recrystallization generally provided by the deformation energy storage of the twisted metal. When the strain rate is low, the metal atoms can fully diffuse and the stored energy in the eutectic microstructure layer is small, so that the driving force of recrystallization is reduced and the nucleation rate of recrystallization is low. At a higher strain rate, a large number of dislocations and structural defects are formed in α-Al, and the deformation storage energy increases, which provides favorable nucleation sites and increases the nucleation rate. As the strain rate increases, the deformation time will decrease accordingly, and the dynamic recrystallization grains do not have enough time to grow up, so the grain size will decrease with the increase of strain rate. With the increase of strain rate, the flow stress of the eutectic microstructure layer increases, which leads to the increase of fragmentation degree of the $CuAl_2$ phase.

3.3. True stress–true strain curve

The true stress–true strain curves of the eutectic microstructure layer under different deformation conditions are shown in Fig. 6. At the initial stage of elastic deformation, the true stress of the eutectic microstructure layer increases linearly with the increase of true strain. Plastic deformation occurs when the stress exceeds the yield strength of the eutectic microstructure layer, the true stress of the eutectic microstructure layer increases slowly with the increase of true strain. Mechanical sclerification caused by dislocation and

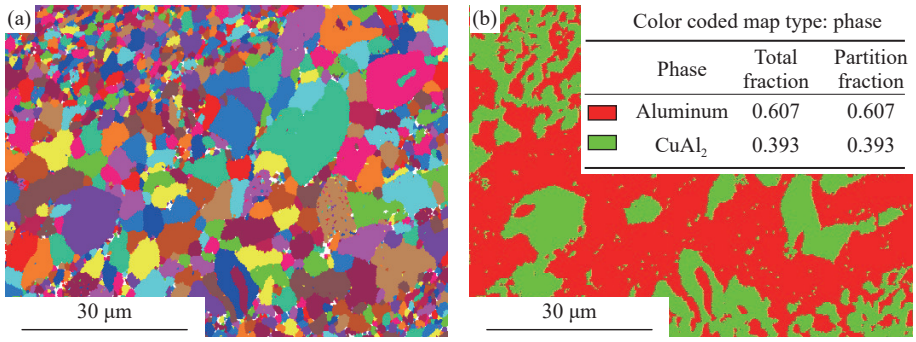

Fig. 4. Microstructure of the eutectic microstructure layer after compression and deformation at 350°C and 0.01 s^{-1}: (a) grain figure; (b) phase diagram.

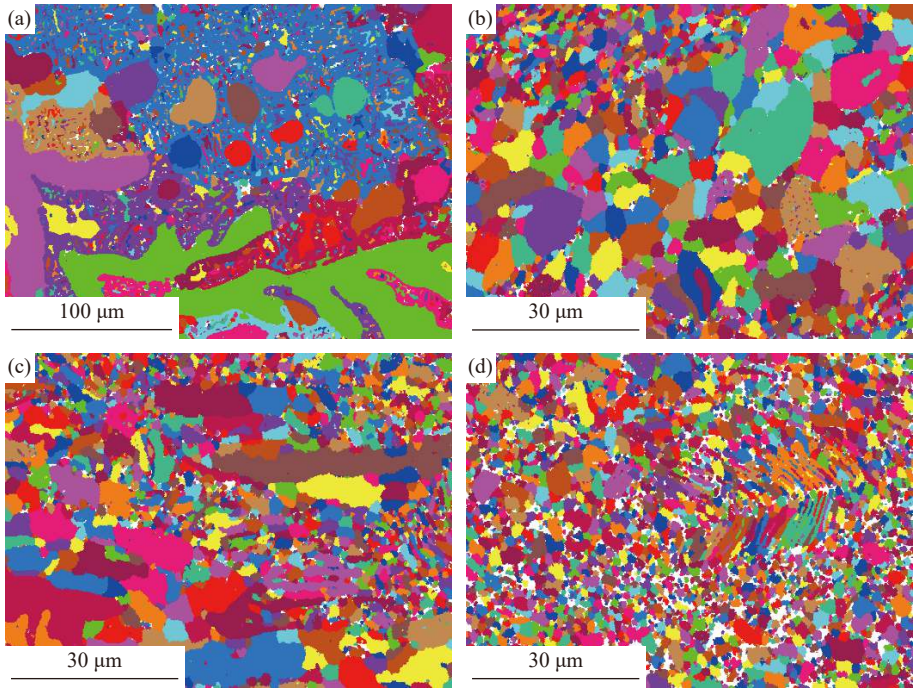

Fig. 5. Microstructure of eutectic microstructure layer after compression deformation under different strain rates at 350°C: (a) original condition; (b) 0.01 s^{-1}; (c) 0.1 s^{-1}; (d) 1 s^{-1}.

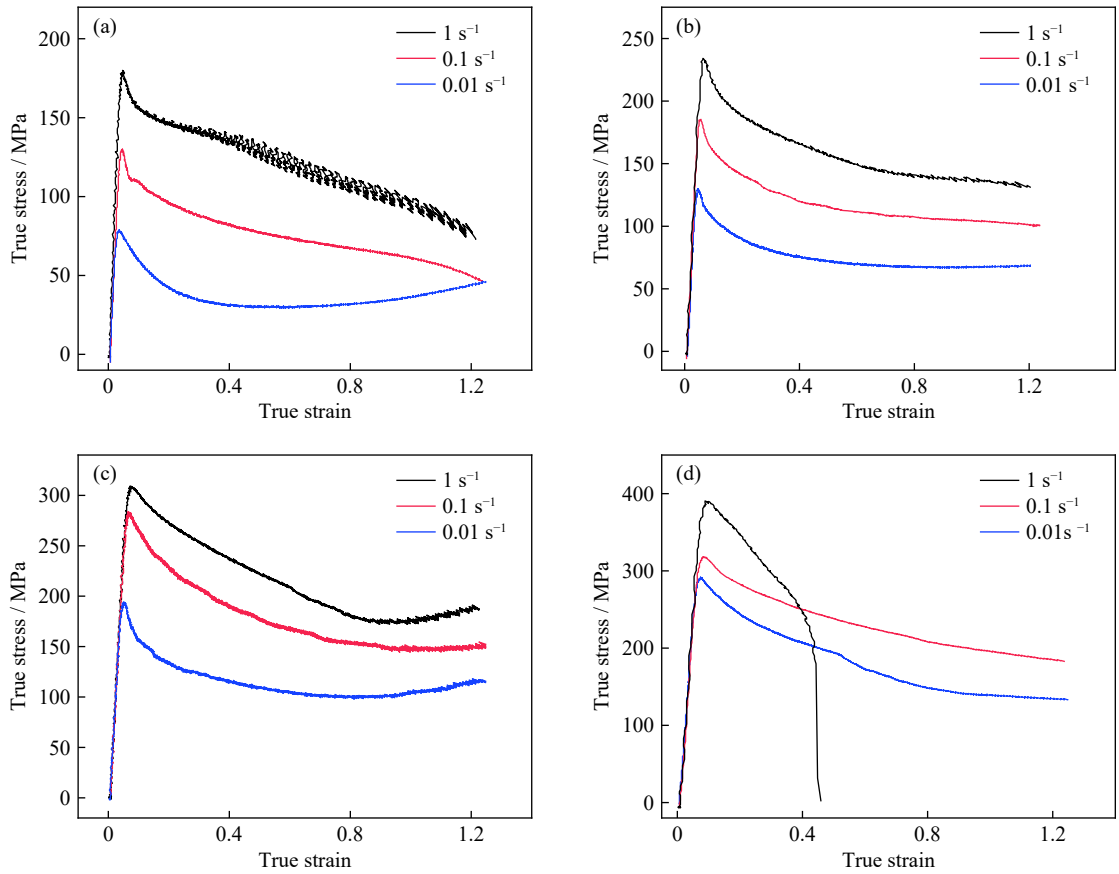

Fig. 6. True stress–true strain curves of eutectic microstructure layer at different deformation temperatures of (a) 400, (b) 350, (c) 300, and (d) 250°C.

mollification caused by dynamic recovery and dynamic recrystallization occur simultaneously in the eutectic microstructure layer of compound interface in this stage. However, because the sclerification caused by high density dislocation in the process of deformation is greater than the mollification caused by dynamic recovery and dynamic recrystallization, the true stress of eutectic microstructure layer on the compound interface increases slowly with the increase of true strain. The true stress declines rapidly after it gets peak, due to the softening effect caused by dynamic recrystallization, which is higher than the work hardening effect. With the continuous increase of true strain, work hardening and dynamic softening compete with each other. Steady rheological characteristics appear when they reach the equilibrium state.

When the deformation temperature is 250°C and the strain rate is 1 s^{-1}, dynamic recrystallization begins when the strain of the eutectic microstructure layer reaches the critical recrystallization strain (ε_c). However, due to the low deformation temperature and high strain rate, the dynamic recrystallization softening is not enough to offset the working hardening, and the eutectic microstructure layer is fractured. A little plastic deformation occurs in the eutectic microstructure layer before fracture, which is consistent with the fracture analysis.

As can be seen from Fig. 6, when the strain rate is constant, the flow stress of the eutectic microstructure layer decreases with the increase of deformation temperature. The effects of increasing deformation temperature on reducing flow stress are mainly as follows: (1) The degree of thermal motion of atoms is significantly enhanced, the critical shear stress required to start the dislocation is obviously reduced, and the number of dislocation slip system is increased, which is beneficial to the plastic deformation of the eutectic microstructure layer. (2) It is helpful to promote the dynamic recrystallization of the eutectic microstructure layer and reduce the degree of work hardening.

3.4. Modeling the hot deformation behavior

3.4.1. Peak stress constitutive model

In order to predict the hot deformation behavior of the eutectic microstructure layer, the thermal compression process was further explored, and the constitutive relation equation of the eutectic microstructure layer was established. The hyperbolic sinusoidal constitutive equation of Arrhenius type is widely used to describe the relationship between the flow stress (peak stress), deformation temperature, and strain rate [22]:

$$\dot{\varepsilon} = A[\sinh(\alpha\sigma)]^n \exp(-\frac{Q}{RT}) \quad (1)$$

where $\dot{\varepsilon}$ is the strain rate, s^{-1}; A, α, and n are material constants; σ is the peak stress, MPa; Q is the deformation activation energy, kJ·mol^{-1}; R is the gas constant, 8.314 J·mol^{-1}·K^{-1}; T is the deformation temperature, K.

In order to obtain each coefficient in the equation, the hyperbolic sinusoidal constitutive equation of the Arrhenius type is simplified as follows:

$$\dot{\varepsilon} = A_1\sigma^{n_1}\exp\left(-\frac{Q}{RT}\right), (\alpha\sigma < 0.8) \tag{2}$$

$$\dot{\varepsilon} = A_2\exp(\beta\sigma)\exp\left(-\frac{Q}{RT}\right), (\alpha\sigma > 1.2) \tag{3}$$

$$\beta = n_1\alpha \tag{4}$$

The logarithm of both sides of Eqs. (2) and (3):

$$\ln\dot{\varepsilon} = \ln A_1 + n_1\ln\sigma - \frac{Q}{RT} \tag{5}$$

$$\ln\dot{\varepsilon} = \ln A_2 + \beta\sigma - \frac{Q}{RT} \tag{6}$$

Fig. 7(a) and (b) shows the peak stress of the eutectic microstructure layer at different deformation temperatures to draw the relationships of $\ln\dot{\varepsilon}$ vs. $\ln\sigma$ and $\ln\dot{\varepsilon}$ vs. σ. Then, the curves are treated with unary linear regression, and their slopes are n_1 and β, respectively. The average n_1 is 7.276, and β is 0.0413 MPa^{-1}. According to Eq. (4), the value of α is 0.0056 MPa^{-1}.

The relationship between temperature compensated strain rate (Z) and peak stress is as follows [23]:

$$Z = \dot{\varepsilon}\exp\left(-\frac{Q}{RT}\right) = A[\sinh(\alpha\sigma)]^n \tag{7}$$

According to the partial derivative for the logarithm of both sides of Eq. (7), the thermal deformation activation energy (Q) is obtained:

$$Q = 1000R\left\{\frac{\partial\ln\dot{\varepsilon}}{\partial\ln[\sinh(\alpha\sigma)]}\right\}_T\left\{\frac{\partial\ln[\sinh(\alpha\sigma)]}{\partial(1/T)}\right\}_{\dot{\varepsilon}} \tag{8}$$

Substitute α in, draw the $\ln\dot{\varepsilon}$ vs. $\ln[\sinh(\alpha\sigma)]$ and $\ln[\sinh(\alpha\sigma)]$ vs. $1000/T$ diagrams, and make linear regression, as shown in Fig. 7(c) and (d). According to the coefficients in Eq. (1): $A = 6.41 \times 10^{12}$ s^{-1}, $\alpha = 0.0056$ MPa^{-1}, $n = 5.41$, and $Q = 1.71 \times 10^5$ $J\cdot mol^{-1}$, the constitutive equation is established as follows:

$$\dot{\varepsilon} = 6.41\times10^{12}[\sinh(0.0056\sigma)]^{5.41}\exp(-\frac{171000}{RT}) \tag{9}$$

By the transformation of Eq. (7), the following equation can be obtained:

$$\sigma = \frac{1}{\alpha}\ln\left\{\left(\frac{Z}{A}\right)^{\frac{1}{n}} + \left[\left(\frac{Z}{A}\right)^{\frac{2}{n}} + 1\right]^{\frac{1}{2}}\right\} \tag{10}$$

The deformation temperature and strain rate under different conditions are substituted into Eqs. (7) and (10) to obtain the theoretical peak stress under the corresponding deformation conditions, and the theoretical peak stress and the experimental peak stress are plotted as discrete points on the ordinate and abscisic coordinates respectively, as shown in Fig. 8. The consistency can be illustrated by Fig. 8: the slope of the straight line obtained by fitting the discrete points is 1.029 and the correlation coefficient is 0.974, which indicates that the peak stress calculated by the constitutive equation is in good agreement with the experimental value, so the obtained constitutive equation is reasonable.

3.4.2. Flow stress constitutive equation

The α, Q, n, and $\ln A$ values at different stresses (ε = 0.2–1.0, an interval is 0.1) were calculated according to the peak stress constitutive equation. After analysis, there is a

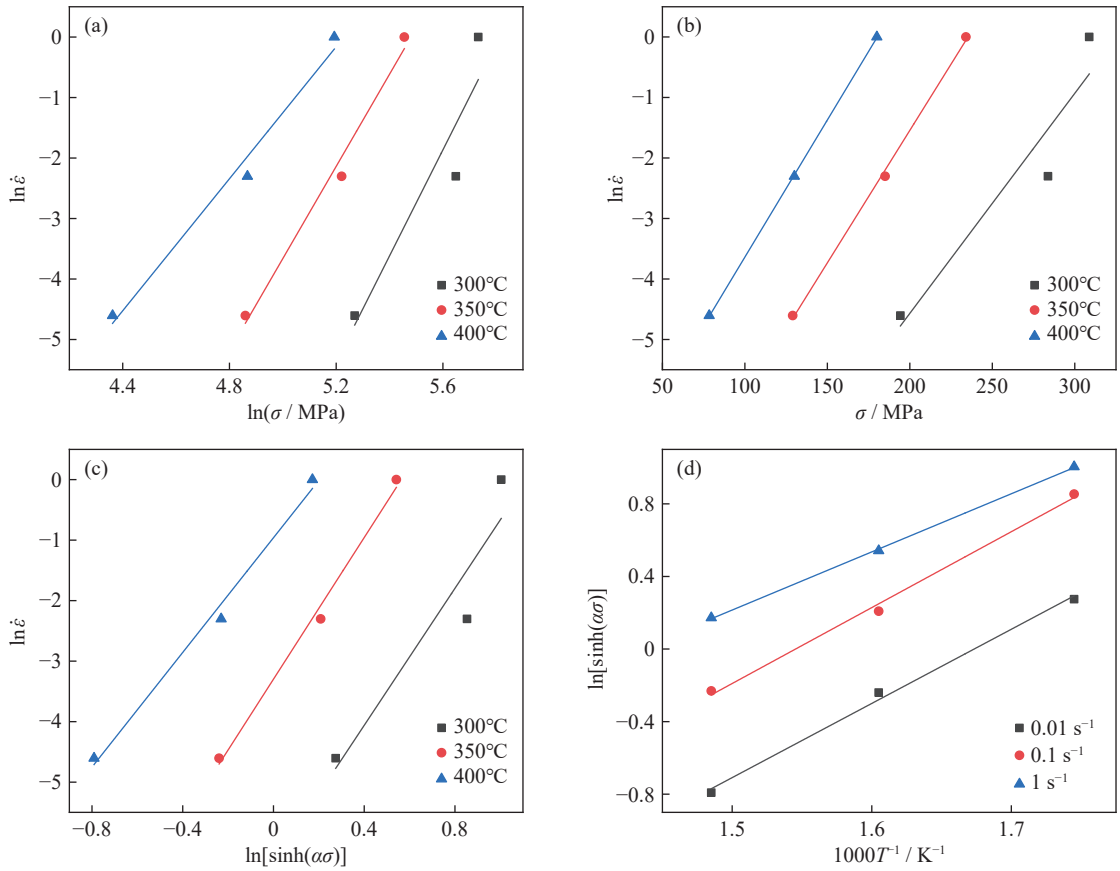

Fig. 7. (a) $\ln\dot{\varepsilon}$ vs. $\ln\sigma$, (b) $\ln\dot{\varepsilon}$ vs. σ, (c) $\ln\dot{\varepsilon}$ vs. $\ln[\sinh(\alpha\sigma)]$, and (d) $\ln[\sinh(\alpha\sigma)]$ vs. $1000/T$ plots at different deformation rates.

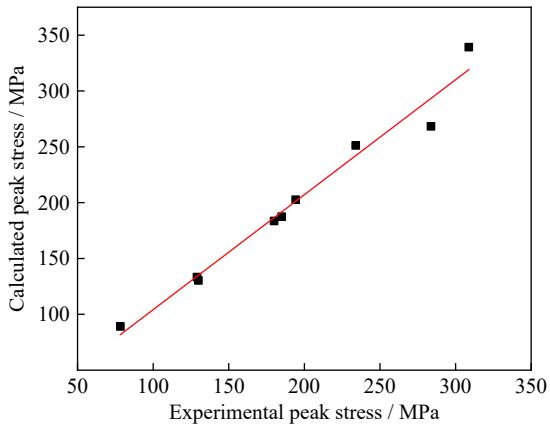

Fig. 8. Relationship between experimental peak stress and calculation peak stress of eutectic microstructure layer.

specific functional relationship between the calculated material parameters and the true strain. The cubic polynomial is used to fit the functional relationship between them, and the fitting effect is good, with the correlation coefficient reaching above 0.98. The variation relationships of material parameters determined by the above method with strain are shown in Fig. 9. The cubic function relations of material parameters with strain are obtained as follows:

$$\alpha = 0.0084\varepsilon^3 + 0.0099\varepsilon^2 + 0.00204\varepsilon + 0.0077 \quad (11)$$

$$n = -1.85712\varepsilon^3 + 6.61381\varepsilon^2 - 4.41095\varepsilon + 4.27135 \quad (12)$$

$$Q = 30306.5\varepsilon^3 + 95834.96\varepsilon^2 - 123995.44\varepsilon + 170445.6 \quad (13)$$

$$\ln A = 6.27438\varepsilon^3 + 17.91655\varepsilon^2 - 24.09948\varepsilon + 29.72358 \quad (14)$$

By the transformation of Eq. (1), the flow stress constitutive equation of the eutectic microstructure layer is obtained as follows:

$$\sigma = \frac{1}{\alpha}\operatorname{arcsinh}\left[\exp\left(\frac{\ln\dot{\varepsilon} - \ln A + \frac{Q}{RT}}{n}\right)\right] \quad (15)$$

where α, n, Q, and $\ln A$ are determined by Eqs. (11)–(14), respectively.

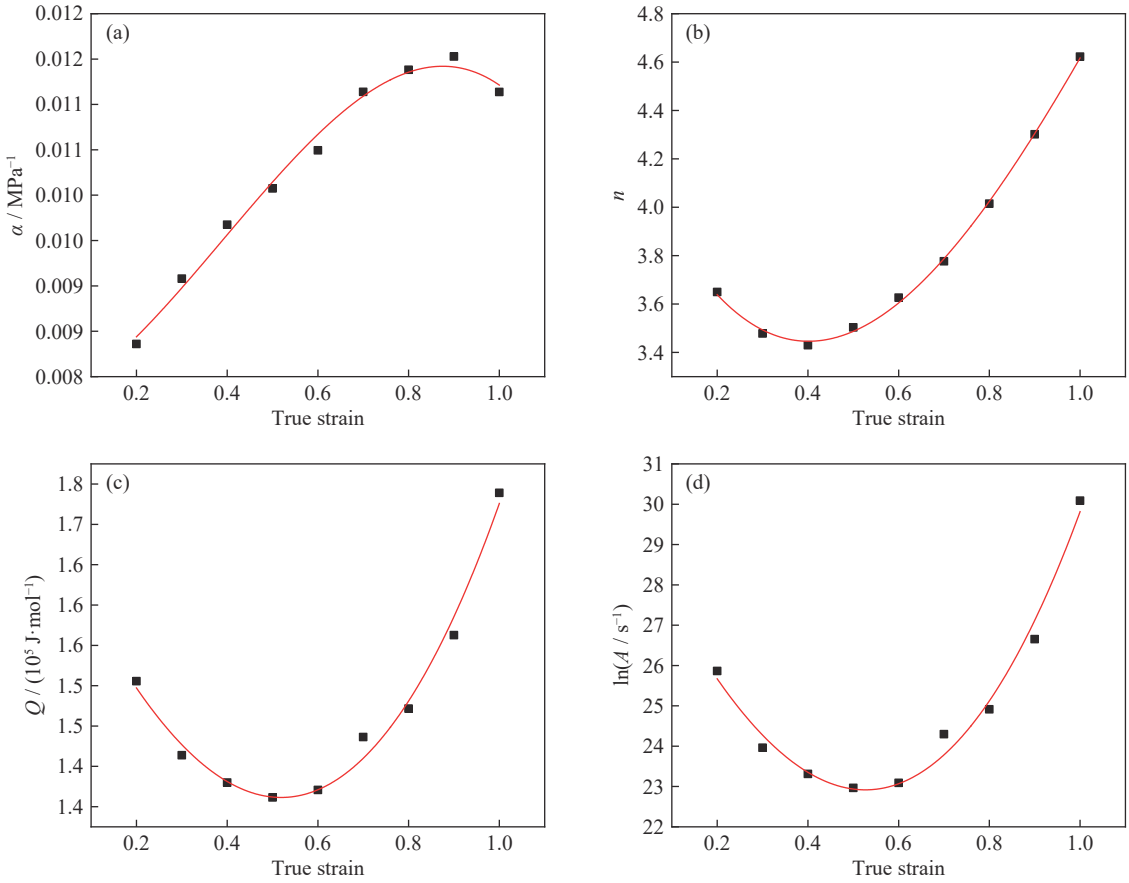

Fig. 9. Relationships between (a) α, (b) n, (c) Q, and (d) $\ln A$ with true strain.

3.4.3. Verification of the flow stress constitutive equation

In order to verify the validity of the established flow stress constitutive equation, the parameters of different deformation temperatures and strain rates under different true strain conditions are substituted into Eq. (15). A total of 81 groups of data are compared between the calculated values of flow stress and the experimental values of flow stress, and the correlation and average absolute relative error are used for verification.

The correlation coefficient is usually used to analyze the linear relationship between experimental values and calculated values. The correlation between the flow stress predicted by the constitutive relation and the experimental value is shown in Fig. 10. It can be seen that the calculated value of

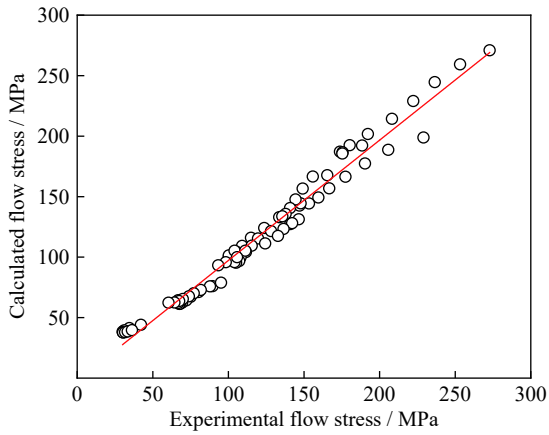

Fig. 10. Relationship between experimental flow stress and calculation flow stress of eutectic microstructure layer.

the constitutive relation has a good correlation with the experimental value, and the correlation coefficient is about 0.978. In order to describe the accuracy of constitutive relation, the average absolute relative error (δ) is introduced [24]:

$$\delta = \frac{1}{N}\sum_{i=1}^{N}\left|\frac{E_i - P_i}{E_i}\right| \times 100\% \tag{16}$$

where E_i is the experimental value of flow stress, P_i is the calculated value by the constitutive relation (Eq. (15)), and N is the number of experimental data points (in this paper $N = 81$). By calculating the deviation of the experimental range, the average absolute relative error is 5.36%. The results show that the eutectic composite interfacial stress obtained by Eq. (15) has high precision and meets the needs of engineering calculation.

The comparison between the calculated values of flow stress and experimental values of flow stress at different deformation temperatures is shown in Fig. 11. It can be seen from the figure that the calculated value of flow stress within the experimental range is almost consistent with the experimental value. This indicated that the model of the eutectic microstructure layer flow stress prediction has a good predictive ability.

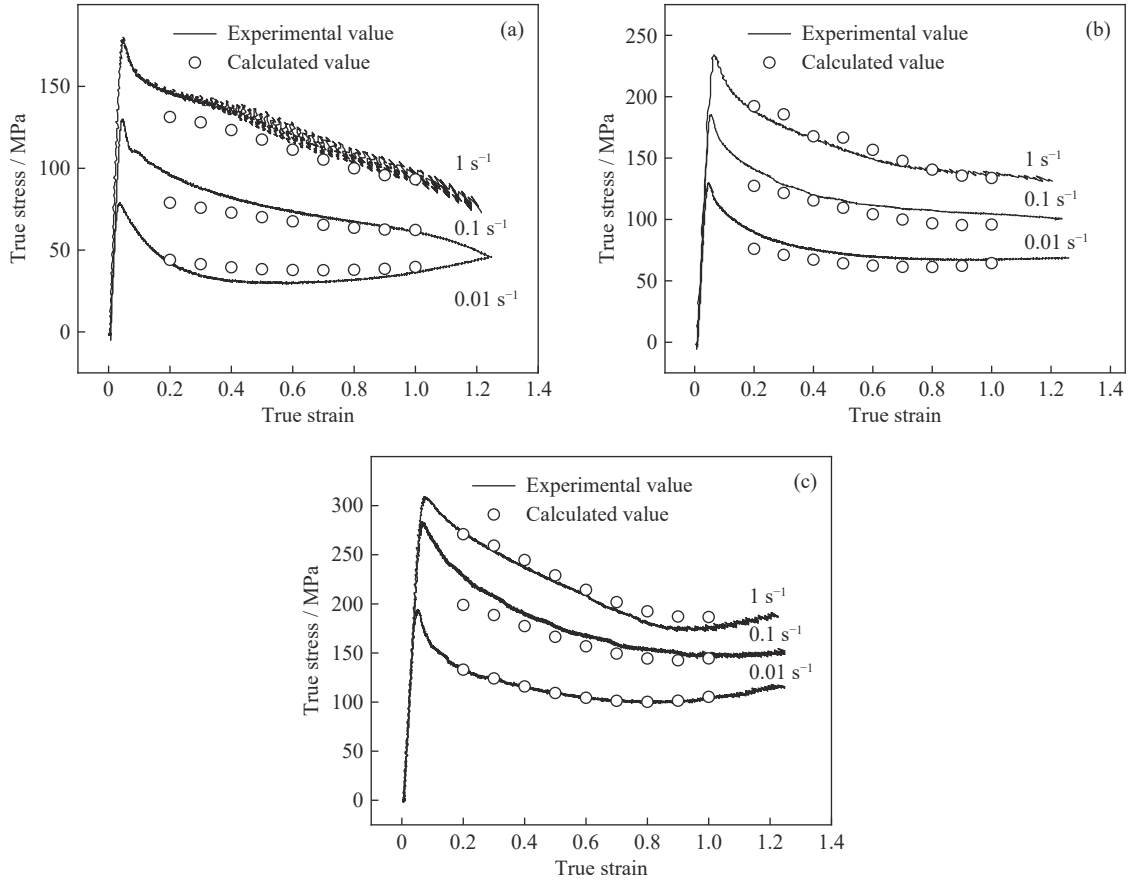

Fig. 11. Comparison between the experimental and calculated flow stress of eutectic microstructure at different deformation temperatures: (a) 400, (b) 350, and (c) 300°C.

3.5. Rheological behavior of composite interface during hot compression of the Cu–Al composites plate

A ϕ8 mm × 15 mm cylindrical sample was taken from the Cu–Al composites plate, as shown in Fig. 12(a). The hot compression test was carried out at the deformation temperature of 300°C and strain rate of 1 s^{-1}, the total deformation was 70%. The composite interface morphology after hot compression is shown in Fig. 12(b) and (c).

As can be seen from Fig. 12(b), during the compression process of the Cu–Al composites plate, the eutectic microstructure in the composite interface undergoes significant plastic deformation, and the deformation thickness is 75.7 μm. The total deformation is 78% compared with the origin-

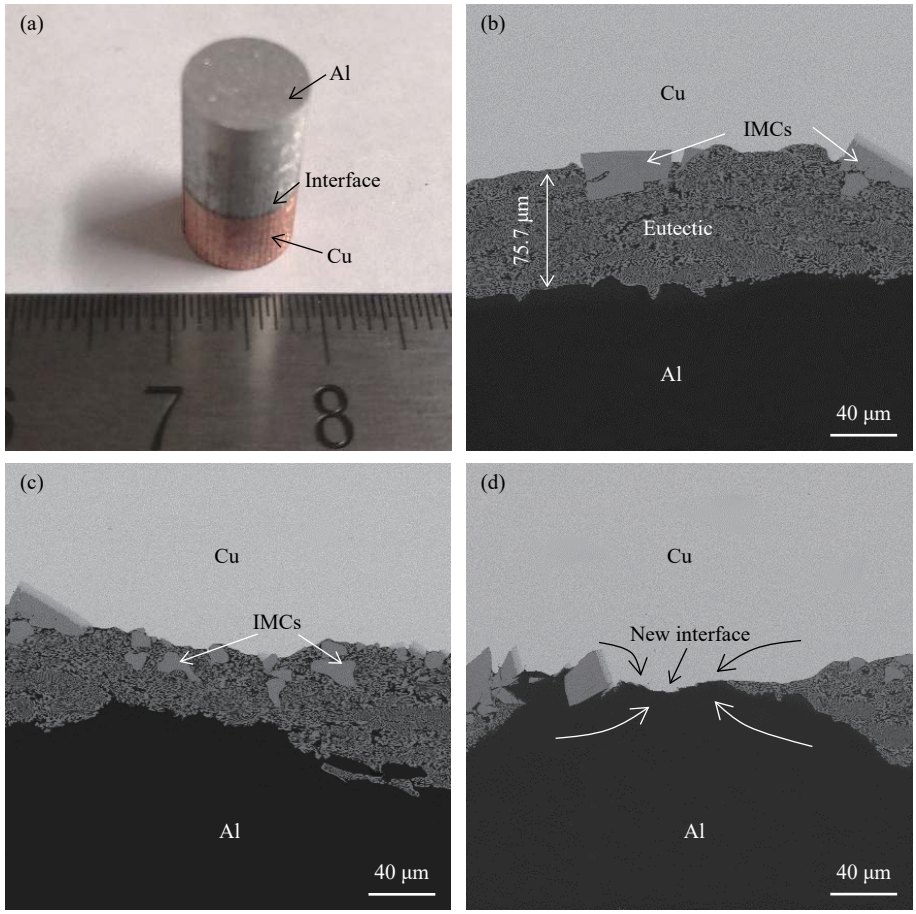

Fig. 12. (a) Cylindrical composite and (b–d) composite interface morphology of the Cu–Al composite after the hot compression deformation.

al thickness. The results show that the eutectic microstructure in the composite interface has plastic deformation behavior during the hot deformation of the Cu–Al composites plate. However, intermetallic compounds (IMCs), which have little plastic deformation capacity, are broken when the stress exceeds their fracture strength. Under the flow behavior of copper and the eutectic microstructure, the IMCs are dispersed in the copper and eutectic microstructure. Due to the non-uniform deformation of copper and aluminum, a large shear force is formed on the composite interface, which causes the composite interface to fracture at a local position, as shown in Fig. 12(c). Under the compressive stress, the fresh copper and aluminum metal flow into the gap and form a new atomic-scale composite interface (Fig. 12(d)), so that the Cu–Al composites plate has a high bonding strength, and the cooperative deformation of Cu–Al composites plate is realized. Therefore, the deformation behavior of the composite interface is the key factor during the forming process of the Cu–Al composites plate.

4. Conclusions

In this paper, Al–17at% Cu alloy, which had the same eutectic structure as the eutectic microstructure layer on the interface of Cu–Al composite plate, was prepared by changing the cooling rate of ingot solidification to substitute the eutectic microstructure layer on the interface of Cu–Al composite plate, and the compression deformation behavior was investigated. The conclusions are as follows:

(1) When the deformation temperature ranges from 300 to 400°C, the softening effect of dynamic recrystallization of α-Al in the eutectic microstructure layer is greater than the hardening effect, and then the uniform plastic deformation of eutectic microstructure is caused.

(2) According to the true stress–strain curves of the eutectic microstructure layer in different deformation conditions, the relationships between true strain and material parameters were obtained by polynomial fitting based on the Arrhenius hyperbolic sinusoid model, and the constitutive equation of flow stress in the eutectic microstructure layer was established:

$$\dot{\varepsilon} = A[\sinh(\alpha\sigma)]^n \exp(-\frac{Q}{RT})$$

where:

$$\alpha = 0.0084\varepsilon^3 + 0.0099\varepsilon^2 + 0.00204\varepsilon + 0.0077,$$

$$n = -1.85712\varepsilon^3 + 6.61381\varepsilon^2 - 4.41095\varepsilon + 4.27135,$$

$$Q = 30306.5\varepsilon^3 + 95834.96\varepsilon^2 - 123995.44\varepsilon + 170445.6,$$

$$\ln A = 6.27438\varepsilon^3 + 17.91655\varepsilon^2 - 24.09948\varepsilon + 29.72358.$$

(3) The correlation coefficient between the experimental value and the calculated value predicted by the constitutive relation is about 0.978, with an average relative error of 5.36%. The accuracy of the constitutive equation of flow

stress in the eutectic microstructure layer established in this paper was verified, which can provide a reliable theoretical basis for rolling forming of the Cu–Al composite plate.

Acknowledgements

This work was financially supported by the National Key Research and Development Program of China (No. 2018YFA0707303) and the National Natural Science Foundation for Distinguished Young Scholars of China (No. 51925401).

Conflict of Interest

The authors declare that they have no known competing financial interests or personal relationships that could have appeared to influence the work reported in this paper.

References

[1] T. Liu, P. Liu, and Q.D. Wang, Research progress on copper/aluminum bimetal composite, *Mater. Rev.*, 27(2013), No. 19, p. 1.

[2] S.Y. Liu, A.Q. Wang, S.J. Lyu, and H.W. Tian, Interfacial properties and further processing of Cu/Al laminated composite: A review, *Mater. Rev.*, 32(2018), No. 5, p. 828.

[3] Y.J. Su, X.H. Liu, Y.F. Wu, H.Y. Huang, and J.X. Xie, Numerical simulation of temperature field in horizontal core-filling continuous casting for copper cladding aluminum rods, *Int. J. Miner. Metall. Mater.*, 20(2013), No. 7, p. 684.

[4] H.M. Xia, L. Zhang, Y.C. Zhu, N. Li, Y.Q. Sun, J.D. Zhang, and H.Z. Ma, Mechanical properties of graphene nanoplatelets reinforced 7075 aluminum alloy composite fabricated by spark plasma sintering, *Int. J. Miner. Metall. Mater.*, 27(2020), No. 9, p. 1295.

[5] R.Y. Feng, W.X. Wang, Z.F. Yan, D.H. Wang, S.P. Wan, and N. Shi, Fatigue limit assessment of a 6061 aluminum alloy based on infrared thermography and steady ratcheting effect, *Int. J. Miner. Metall. Mater.*, 27(2020), No. 9, p. 1301.

[6] Z.H. Deng, H.Q. Yin, X. Jiang, C. Zhang, G.F. Zhang, B. Xu, G.Q. Yang, T. Zhang, M. Wu, and X.H. Qu, Machine-learning-assisted prediction of the mechanical properties of Cu–Al alloy, *Int. J. Miner. Metall. Mater.*, 27(2020), No. 3, p. 362.

[7] M.M.H. Athar and B. Tolaminejad, Weldability window and the effect of interface morphology on the properties of Al/Cu/Al laminated composites fabricated by explosive welding, *Mater. Des.*, 86(2015), p. 516.

[8] M.M. Hoseini-Athar and B. Tolaminejad, Interface morphology and mechanical properties of Al–Cu–Al laminated composites fabricated by explosive welding and subsequent rolling process, *Met. Mater. Int.*, 22(2016), No. 4, p. 670.

[9] T. Wang, S. Li, Z.K. Ren, J.C. Han, and Q.X. Huang, A novel approach for preparing Cu/Al laminated composite based on corrugated roll, *Mater. Lett.*, 234(2019), p. 79.

[10] L. Li, K. Nagai, and F.X. Yin, Progress in cold roll bonding of metals, *Sci. Technol. Adv. Mater.*, 9(2008), No. 2, art. No. 023001.

[11] X.B. Li, G.Y. Zu, and P. Wang, Microstructural development and its effects on mechanical properties of Al/Cu laminated composite, *Trans. Nonferrous Met. Soc. China*, 25(2015), No. 1, p. 36.

[12] W.M. Jiang, F. Guan, G.Y. Li, H.X. Jiang, J.W. Zhu, and Z.T. Fan, Processing of Al/Cu bimetal via a novel compound casting method, *Mater. Manuf. Processes*, 34(2019), No. 9, p. 1016.

[13] F. Guan, W.M. Jiang, G.Y. Li, H.X. Jiang, J.W. Zhu, and Z.T. Fan, Interfacial bonding mechanism and pouring temperature effect on Al/Cu bimetal prepared by a novel compound casting process, *Mater. Res. Express*, 6(2019), No. 9, art. No. 096529.

[14] S.Y. Liu, A.Q. Wang, H.W. Tian, and J.P. Xie, The synergetic tensile deformation behavior of Cu/Al laminated composites prepared by twin-roll casting technology, *Mater. Res. Express*, 6(2018), No. 1, art. No. 016530.

[15] W.K. Lu, J.P. Xie, A.Q. Wang, J.W. Li, and Y.D. Zhang, Effects of annealing temperature on interfacial microstructure and mechanical properties of Cu/Al roll-casted composite plate, *Mater. Mech. Eng.*, 38(2014), No. 3, p. 14.

[16] J. Wang, Y. Lei, X.H. Liu, G.L. Xie, Y.Q. Jiang, and S. Zhang, Microstructure and properties of Cu–Al-laminated composites fabricated via formation of a horizontal casting composite, *Chin. J. Eng.*, 42(2020), No. 2, p. 216.

[17] Y.J. Su, X.H. Liu, H.Y. Huang, C.J. Wu, X.F. Liu, and J.X. Xie, Effects of processing parameters on the fabrication of copper cladding aluminum rods by horizontal core-filling continuous casting, *Metall. Mater. Trans. B*, 42(2011), No. 1, p. 104.

[18] Y.F. Wu and X.H. Liu, FE simulation of rolling for copper cladding aluminum with rectangle section, *J. Plast. Eng.*, 22(2015), No. 6, p. 91.

[19] J.Y. Li, J.T. Luo, J.L. Shen, and Y.F. Gu, Roll deformation process simulation and rolling force calculation formula of copper clad aluminum composites, *Acta Mater. Compos. Sin.*, 31(2014), No. 6, p. 1551.

[20] Y.B. Luo, X.Y. Dai, and J. Zhang, Numerical simulation and experimental investigation on rolling deformation strain of copper cladding aluminum flat wires, *Mater. Rev.*, 28(2014), No. 8, p. 157.

[21] S.Y. Liu, A.Q. Wang, T.T. Liang, and J.P. Xie, Hot deformation behavior of Cu/Al laminated composites under interface constraint effect, *Mater. Res. Express*, 5(2018), No. 6, art. No. 066531.

[22] W.Y. Wang, Q.L. Pan, Y.W. Sun, X.D. Wang, A.D. Li, and W.B. Song, Study on hot compressive deformation behaviors and corresponding industrial extrusion of as-homogenized Al–7.82Zn–1.96Mg–2.35Cu–0.11Zr alloy, *J. Mater. Sci.*, 53(2018), No. 16, p. 11728.

[23] C. Zener and J.H. Hollomon, Problems in non-elastic deformation of metals, *J. Appl. Phys.*, 17(1946), No. 2, p. 69.

[24] B. Zhang, L.L. Zhu, K.S. Wang, W. Wang, and Y.X. Hao, High temperature plastic deformation behavior and constitutive equation of pure nickel, *Chin. J. Rare Met.*, 39(2015), No. 5, p. 406.